

Building blocks of a scalable and radiation-hardened integrated transmitter unit based on 250 nm SOI

Y. Zhang *, M. Schneider, D. Karnick, L. Eisenblätter, T. Kühner, M. Weber
Karlsruhe Institute of Technology, Institute for Data Processing and Electronics,
Hermann-von-Helmholtz-Platz 1, 76344 Eggenstein-Leopoldshafen, Germany

ABSTRACT

One promising solution for the ever increasing transmission capacity demand from fundamental research and data centers is the silicon-photonic integrated WDM transmitter. We designed an easily scalable, high-bandwidth transmitter unit composed of radiation-hardened Mach-Zehnder modulators (MZMs) and Echelle grating (de-)multiplexers (EG-DMUXs).

Our 3 mm MZMs have customized slabs with a reduced etch depth to improve their radiation hardness. Our current MZMs feature a $V_{\pi} \cdot L$ of 4.6 V·cm and an insertion loss of 4.84 dB. Additionally, an error-free transmission was achieved successfully at a speed of 11.3 Gb/s while driving the modulators with a PRBS-7 signal and an amplitude of less than $2 V_{pp}$.

The Echelle grating (de-)multiplexers were designed and simulated numerically. The presented 1×7 device is compact and low-loss: the on-chip footprint is $680 \mu\text{m} \times 380 \mu\text{m}$, the channel spacing is 800 GHz, and the measured average insertion loss and crosstalk are 2.5 dB and -22 dB, respectively. With optimized components, higher bandwidth systems with more channels are achievable.

Keywords: Mach-Zehnder modulator (MZM), Echelle grating de-/multiplexer (EG-DMUX), wavelength division multiplexing (WDM), silicon on insulator (SOI), integrated transmitter.

1. INTRODUCTION

The data throughput of large data centers in the future will increase exponentially [1]. To meet with human beings' ever increasing demands on higher-quality communication and data storage, a novel faster transmission system is urgently required instead of installing more optical fibers and building more large-scale infrastructures. A similar challenge exists in the fundamental research as well. For instance, the Europe Organization for Nuclear Research (CERN) is generating large amounts of data in their detectors and the rate will increase to several terabits per second in the future. More importantly, the scientific data originates from the inner detectors where the radiation levels are extremely high. The harsh environment of high radiation levels, low temperatures, strong magnetic fields and fast transmission speed requirements raise the development challenges [2], [3].

In recent years, the research group from CERN published their research on radiation hardened modulators [3] which seems a promising way to solve the irradiation issue. On the other hand, a highly developed fabrication technology for silicon-on-insulator photonics enables compact integrated optical components including grating couplers, modulators, EG-DMUX, and others. We propose a scalable and radiation-hardened integrated transmitter to upgrade the optical data transmission of future detector systems [4]. In this paper, two key building blocks of the transmitter, the MZM [5] and the Echelle grating (de-)multiplexers, will be presented, as well as a fully integrated four channel WDM transmitter.

2. TRANSMITTER CONCEPT

Figure 1 shows the concept of our integrated transmitter in a full setup. The signal from the detector elements will be amplified and preprocessed by the front-end ASICs. Modulator drivers amplify their output signals to meet the requirements of the MZMs. Each channel is connected to an individual MZM on a photonic chip. The photonic chip integrates an Echelle grating demultiplexer, several MZMs and an Echelle grating multiplexer. The inset picture at the left side shows the concept of an MZM. As can be seen, the input signal is divided equally by a 3-dB MMI [6] and linked to two phase shifters. If the two phase shifters are biased differently, light will have different propagating constants and depending on their phase relation at the shifter end, constructive or destructive interference takes places, resulting in an on-off keying

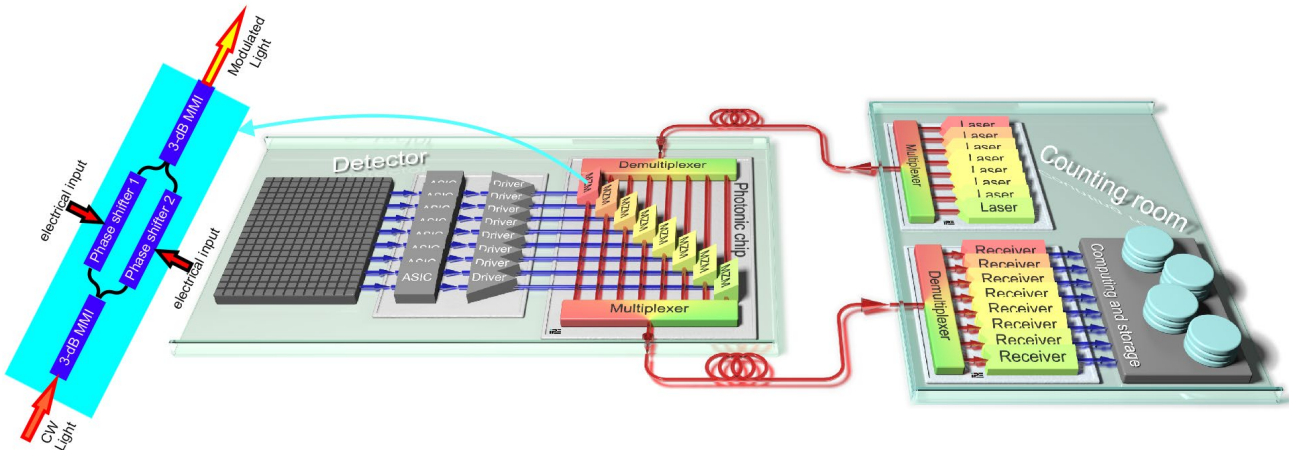


Figure 1. System schematic of the integrated transmitter.

modulation. As the laser sources are located outside the detector volume and the optical carriers are transmitted by a single mode fiber to the photonic chip, radiation will not be an issue for the lasers. The transmission bandwidth per fiber is merely determined by the modulation speed of the modulator and the useable channels of the EG-DMUX.

3. MACH ZEHNDER MODULATORS

The phase shifters in our scheme are 3 mm long and feature a $500 \text{ nm} \times 250 \text{ nm}$ rib geometry as can be seen in Figure 2 as cross section. The silicon is p-type and n-type doped, respectively, with a horizontal pn-junction in the middle of the rib. The doping concentrations of both parts are designed to be in the order of $2.5 \times 10^{17} \text{ cm}^{-3}$. The p+ and n+ sections are highly doped for a good electrical contact between silicon and metal with a doping concentration in the order of 10^{20} cm^{-3} . We made two phase shifter designs with slabs of 120 nm thickness for the standard type and 180 nm thickness for the radiation-hardened type. As shown in [3], the latter design results in a much higher radiation tolerance. On the other hand, the increased thickness of the slab results in a less confined optical mode and a slightly decreased modulation efficiency. Therefore, the etch depth of the slab region should be determined with careful considerations. For the purpose of characterization, the arm lengths of the MZMs were designed asymmetrically so that the operating wavelength is another degree of freedom to set a proper working point. In this way, a voltage-induced wavelength shift ($\Delta\lambda$) measured in the transmission spectrum of the asymmetric MZM can be used to obtain the voltage-induced phase shift according to $\Delta\phi = 2\pi \cdot \Delta\lambda / \text{FSR}$ [7] where FSR is the free spectral range of the asymmetric MZM. As shown in Figure 3, the measured FSR of the radiation-hardened 3-mm asymmetric MZM is 11.5 nm and a wavelength shift of $\Delta\lambda = 1.5 \text{ nm}$ can be achieved by applying a reverse voltage of 4 V. In consequence, the derived $V_{\pi} \cdot L$ is 4.6 V·cm. The measured total insertion loss is

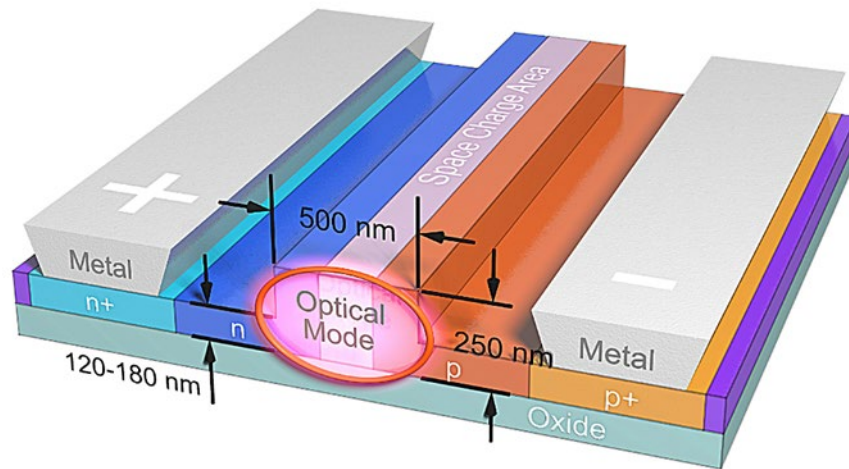


Figure 2. Schematic view of one SOI phase shifter used in the MZMs.

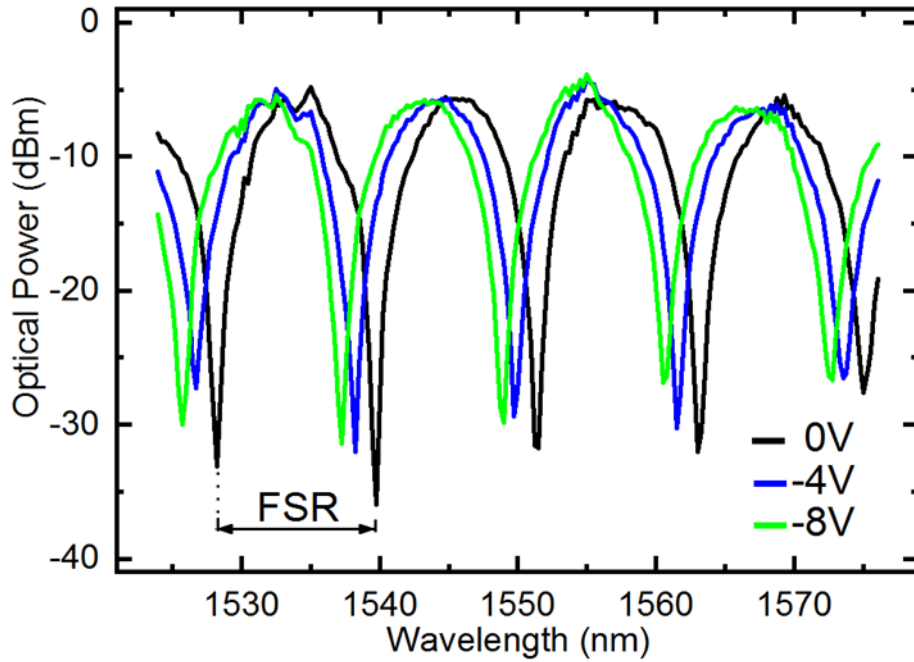


Figure 3. Transmission spectrum of a radiation-hardened, 3-mm asymmetric MZM at different bias voltages.

4.84 dB when the MZM is in the ‘on’ state and the maximum optical transmission occurs. The estimated loss of the MZM is around 1.61 dB/mm. In comparison with the results presented in other literature, the modulation efficiency and insertion loss of our modulators are relatively low. The phenomenon is due to an undesired low doping concentration due to a fabrication problem, which resulted in a doping concentration of the p and n section of both in the order of $6 \times 10^{16} \text{ cm}^{-3}$, four times lower than the intended value.

Although the fabrication error deteriorates the performance of the modulator significantly, we still successfully conducted high-speed performance measurements. The measurement setup is shown in Figure 4: a pseudo-random bit sequence (PRBS) with a length of 2^7-1 bits and a rate of 11.3 Gbit/s was generated by an Altera Stratix V GX FPGA on a Transceiver Signal Integrity Development board. The reverse bias voltages and the RF signal were applied by coplanar probe tips. The optical carrier was generated by a tunable laser source (Agilent 81689A) with a power of 6 dBm. A polarization controller was utilized to maintain TE polarization before the light entered the MZM. The optical output of the modulator was fed into an optical amplifier (EDFA) and a successive optical bandpass filter filtered spontaneous emission noise of the EDFA. With a variable optical attenuator, the average optical power was set to the desired value, which could be measured by a power meter connected to the 10% branch of a 90:10 splitter. The dominant part of the signal was fed into the receiver side of a commercial SFP+ module (Fiberstore SFP-10GER-55). The module could be connected to an oscilloscope for eye diagram measurements or to the FPGA board for bit error rate (BER) measurements.

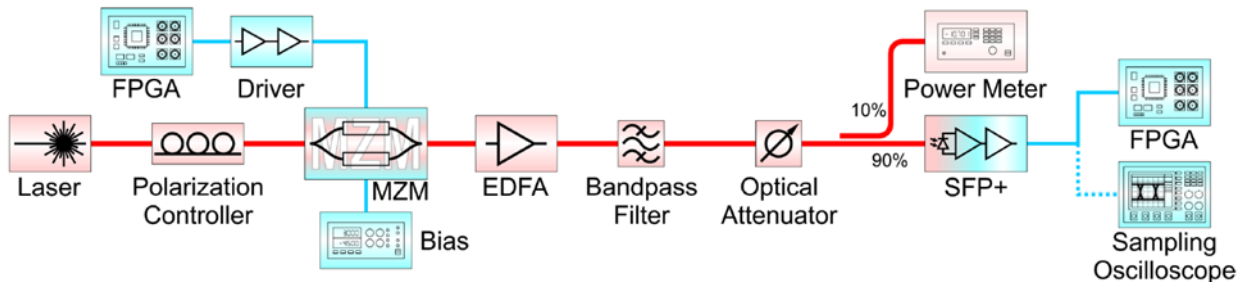


Figure 4. System setup for the high-speed performance measurements.

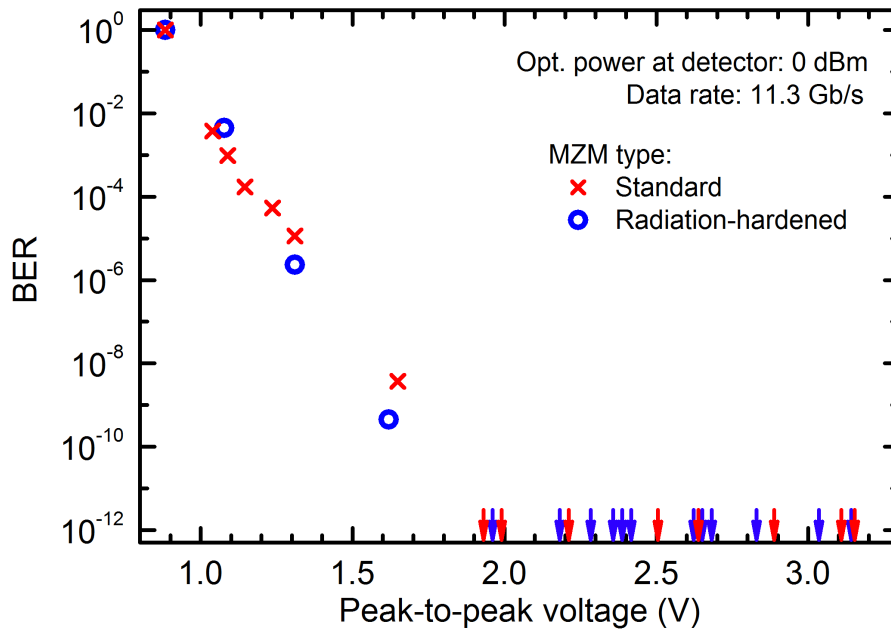


Figure 5. BER measurements at different driving amplitudes for the 3-mm asymmetric MZM.

With the above mentioned measurement setup, we conducted BER measurements at a data rate of 11.3 Gb/s while varying the amplitude of the electrical driving signal for the modulator between $0.88 V_{pp}$ and $3.15 V_{pp}$. The EDFA and the optical attenuator were set to achieve an optical power of 0 dBm at the receiver. For each measurement, at least 6×10^{12} bits were transmitted. As shown in Figure 5 the BER is less than 10^{-12} for both types of modulators when the voltage is larger than $1.9 V_{pp}$. The increase of the BER at lower voltages is very similar for both types.

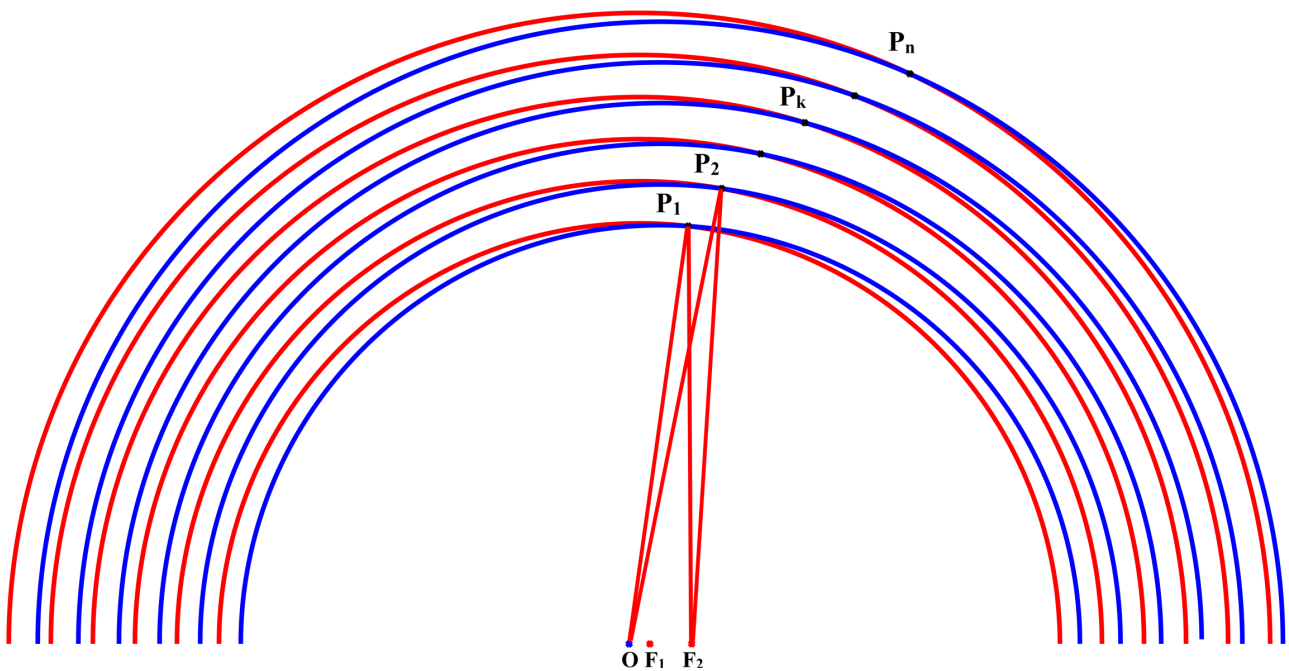


Figure 6. Schematic of an Echelle grating de-multiplexer based on two stigmatic points.

4. ECHELLE GRATING (DE-)MULTIPLEXER

The other key component of an integrated WDM transmitter system is the (de-)multiplexer. Two kinds of (de-)multiplexers were extensively investigated in the SOI platform, the arrayed waveguide grating (AWG) [8] and the Echelle gratings [9]. Compared to AWGs, the Echelle gratings are more tolerant to edge roughness and feature a more compact on-chip footprint. The Echelle gratings presented in this paper are constructed based on two stigmatic points (TSP) [10].

For any ellipse, the relation $|\overline{f_1P} + \overline{f_2P}| = 2a$, stands, where P is a random point on the ellipse, f_1 and f_2 are two foci of the ellipse and $2a$ is a constant. In the following calculation, the input port and two output ports of an EG-DMUX are regarded as three points O , F_1 and F_2 , as shown in Figure 6. Regarding O and F_1 as two foci of an ellipse and $2a = \lambda_{1eff} \cdot m \cdot N$, one can draw a set of ellipses (the blue ones in the figure) where λ_{1eff} is the effective wavelength of the operating wavelength of the output port located at point F_1 , m is the diffraction order and N is a random integer. Similarly, another set of ellipses can be drawn regarding O and F_2 as the foci and $2a = \lambda_{2eff} \cdot m \cdot N$. Consequently, a series of intersections $P_1, P_2, \dots, P_k, \dots, P_n$ are generated. As the optical path difference between any $|\overline{f_1P_n} + \overline{f_2P_n}|$ are integer times of 2π , constructive interference will take place at the output ports for its related operating wavelength. Therefore the intersections are grating points, where reflectors to be placed.

With these considerations we developed a design kit and constructed a compact EG-DMUX with the following parameters: the distances between O , F_1 and F_2 are $|\overline{OF_1}| = 9 \mu\text{m}$ and $|\overline{OF_2}| = 39.8 \mu\text{m}$, respectively, and the diffraction order is $m = 9$. Constant $2a$ ranges from $398 \mu\text{m}$ to $716 \mu\text{m}$ and the device should be fabricated on a 250 nm SOI platform with SiO_2 cladding layers. The designed device has a grating span of 36.8° and an on-chip footprint of about $680 \mu\text{m} \times 360 \mu\text{m}$. The channel spacing is 800 GHz . The seven output ports and the input port are connected to individual out-of-plane grating couplers for the purpose of characterization. Numerical simulations of the design were made using Comsol Multiphysics.

For experimental characterizations, a tuneable laser to generate continuous-wave light around the C band and with a minimum wavelength increment of 0.25 nm was used. TE polarization of the incident light was ensured by a polarization controller. At the receiver side, an optical power meter (Agilent 81618A with 81623B detector head) was used to detect the output light. The simulated and measured transmission spectra are presented in Figure 7. The full lines show the measured data and the dotted curves are the simulation results. As can be seen, the theoretical result and experimental

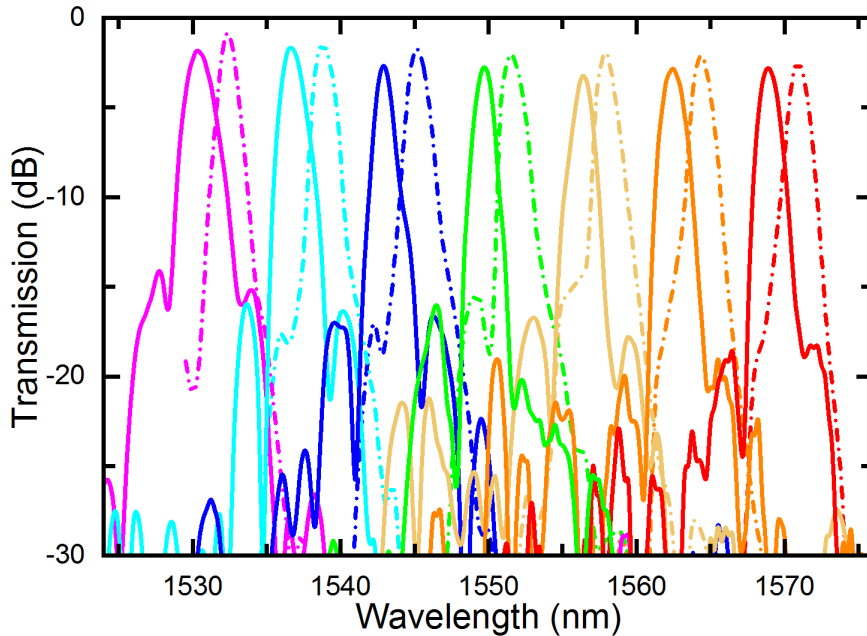


Figure 7. Simulated and measured transmission spectrum of the designed device

result have a good agreement. The device has an average transmission of -2.45 dB for the 7 transmission channels with a maximum value of -1.61 dB and a minimum value of -3.18 dB. The average crosstalk is -22.81 dB with a maximum value of -20.26 dB and a minimum value of -37.69 dB. The wavelengths of the individual channels are blue-shifted by 2 nm, which is mainly due to the refractive index error and one possible source is inaccurate silicon crystalline layer thickness.

5. INTEGRATED 4-CHANNEL TRANSMITTER

Based on the above mentioned building blocks, we designed an integrated 4-channel WDM transmitter. Different from the asymmetric MZM design presented in section 3, the arm lengths here are symmetric for each MZM. In consequence, the working point has to be controlled by the bias voltage of each phase shifter. Additionally, only every other channel of the designed EG-DMUX is used. The transmitter was fabricated on the same 250 nm SOI platform as the other components and a microscope picture of one transmitter is shown in Figure 8. The Echelle gratings (white components) can be seen in the middle of the picture, surrounded by four MZMs with their orange-color coplanar transmission lines for electrical contact. The optical waveguides can hardly be seen as weak dark lines. A full system characterization is not yet available, but the next run of the photonic chip is currently in fabrication, aiming at getting the desired doping concentrations.

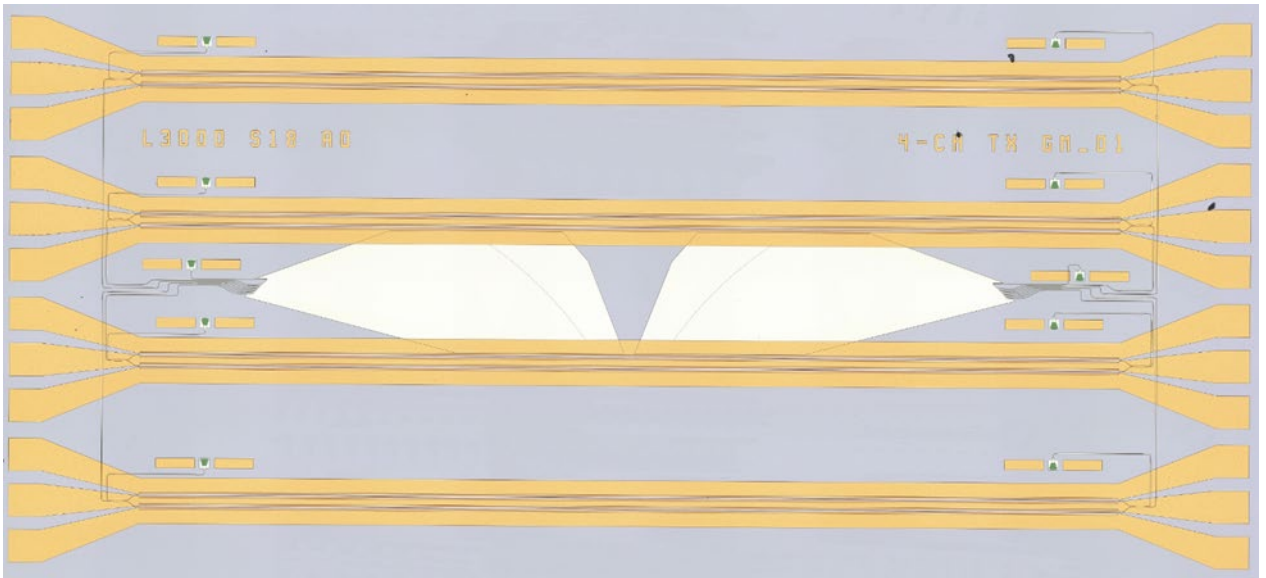


Figure 8. Microscope picture of a 4-channel integrated WDM transmitter.

6. CONCLUSION

In this paper, we presented two key building blocks of a scalable and radiation-hardened integrated transmitter, the MZM and the EG-DEMUX, respectively. The designed MZM features a measured modulation efficiency of $V_{\pi} \cdot L = 4.6 \text{ V} \cdot \text{cm}$, a total insertion loss of 4.84 dB, and an error-free transmission was achieved at a rate of 11.3 Gbit/s for a smallest driving amplitudes of 1.9 V_{pp}. The relatively low modulation efficiency and insertion loss result from an undesired low doping concentration. The presented EG-DEMUX was designed using the TSP method and has a compact on-chip footprint of $680 \mu\text{m} \times 360 \mu\text{m}$, a low insertion loss of 2.45 dB, and a low crosstalk of -22.81 dB. A complete 4-channel integrated WDM transmitter was designed and presented. With the current building blocks and design methods, many more modulators can be integrated into a transmitter. Together with the development of faster modulators in the future, the transmission bandwidth of the integrated transmitter can be improved significantly to revolutionize the data transmission and readout scheme of future detector systems.

7. ACKNOWLEDGEMENT

This research is supported by the program Matter and Technology of the Helmholtz Association, Germany and the China

REFERENCES

- [1] Baldwin P, Gaillard M. "CERN's IT gears up to face the challenges of LHC Run 2." <http://cerncourier.com/cws/article/cern/65031> (2016).
- [2] Troska J, Detraz S, El Nasr-Storey SS, Stejskal P, Sigaud C, Soos C, Vasey F. "Radiation damage studies of lasers and photodiodes for use in multi-Gb/s optical data links." *IEEE Transactions on Nuclear Science* 58.6 (2011): 3103-3110.
- [3] Kraxner A, Detraz S, Olantera L, Scarcella C, Sigaud C, Soos C, Troska J, Vasey F. "Investigation of the Influence of Temperature and Annealing on the Radiation Hardness of Silicon Mach-Zehnder Modulators." *IEEE Transactions on Nuclear Science* 65.8 (2018): 1624-1631.
- [4] Zhang Y, Schneider M, Karnick D, Eisenblätter L, Kühner T, Weber M., "Key building blocks of a silicon photonic integrated transmitter for future detector instrumentation. " *Journal of Instrumentation* 14.08 (2019): P08021.
- [5] Ding J, Chen H, Yang L, Zhang L, Ji R, Tian Y, Zhu W, Lu Y, Zhou P, Min R, Yu M. "Ultra-low-power carrier-depletion Mach-Zehnder silicon optical modulator." *Optics express* 20.7 (2012): 7081-7087.
- [6] Bryngdahl O. "Image formation using self-imaging techniques." *JOSA* 63.4 (1973): 416-419.
- [7] Park JW, You JB, Kim IG, Kim G. "High-modulation efficiency silicon Mach-Zehnder optical modulator based on carrier depletion in a PN Diode." *Optics express* 17.18 (2009): 15520-15524.
- [8] Castellan C, Tondini S, Mancinelli M, Kopp C, Pavesi L., "Low crosstalk silicon arrayed waveguide gratings for on-chip optical multiplexing." *Silicon Photonics: From Fundamental Research to Manufacturing*. Vol. 10686. International Society for Optics and Photonics (2018): DOI: 10.1117/12.2306120.
- [9] Zhang Y, Schneider M, Karnick D, Eisenblätter L, Kühner T, Weber M. "Low-loss and robust DWDM Echelle grating (de-) multiplexers in SOI technology." *Optical Components and Materials XVI*. Vol. 10914. International Society for Optics and Photonics (2019): DOI: 10.1117/12.2507433.
- [10] Horst F, Green WM, Offrein BJ, Vlasov Y. "Echelle grating WDM (de-) multiplexers in SOI technology, based on a design with two stigmatic points." *Silicon Photonics and Photonic Integrated Circuits*. Vol. 6996. International Society for Optics and Photonics (2008): DOI: 10.1117/12.781232.